Efficiency Optimization of Two Dual Active Bridge Converters Operating in Parallel

Michal Rolak, Cezary Sobol, Mariusz Malinowski, *Fellow, IEEE*, and Sebastian Stynski, *Senior Member, IEEE*

***Abstract*—Growing interest in dc-type energy storage systems (ESS) and dc/dc converters has led to increased power ratings of such devices, which often requires parallel connection. The process of energy efficiency optimization of such modular systems is described in literature mainly in terms of the varying power demand, but the problem is more complex and not analyzed yet in relation to varying energy storage (ES) voltage level and bidirectional energy transfer at the same time. Therefore, this article considers the input parallel output parallel (IPOP) connection of two dual active bridge (DAB) modules as a representative modular converter, and to answer a question of: how to improve (maximize) efficiency of such a system, at different power demands and varying ESS voltage, only by a turn ON/OFF operation of the module without any circuit and control algorithm changes. The proposed solution defines an operating area (enclosing different ES's voltage levels and loading power conditions) showing where one or two modules should operate to improve the overall efficiency. A curve fitting approach and polynomial approximation of the single module's input/output power curves are utilized for the proposed algorithm based on parametric functions. After simulation study, the method is validated with two 1.4 kW SiC-based DAB converters, operating at 100 kHz of switching frequency within a wide (0–270 V) ES's voltage range.**

***Index Terms*—Dual active bridge (DAB), energy storage, parallel operation IPOP, optimization.**

I. Introduction

DUE to continuous development of smart grids (SG) an increasing interest in energy storage systems (ESS) is observed [1], [2]. A primary goal of ESS is to provide energy buffers for SGs (with their renewable sources) and utility grids, so they may perform a power smoothing operation [3]. Among many energy storage (ES) solutions such as flywheels, compressed air, pumped water, the dc-type storage systems such as supercapacitors and batteries are of special interest. Additionally, by merging the latter ones an interesting solution has been proposed that results in hybrid energy storage system (HESS) [4], which offers good dynamics, sufficient storing capabilities, and does not require special terrain conditions. This HESS's type may be characterized by a wide-range of voltage changes (from zero to a rated value) when the supercapacitor in parallel active HESS topology is considered. Similarly, the battery-type HESS have varying voltage levels as well, however, in a much narrower range, which depends on the number of batteries connected in series.

To overcome a problem of interfacing different voltage levels in the dc-type ES systems a number of novel topologies has been presented in [5] and [6]. However, still one of the most popular solutions is a typical dual active bridge (DAB) converter [7]. Its wide range of operating voltages, ability of bidirectional energy transfer, and basic phase-shift control make it a simple and suitable choice.

However, when it comes to the increased power rating and physical limitations of DAB's components, this topology can be extended to a three-phase DAB [8], [9] or even a six-leg converter [10]. Another approach, to meet higher power requirements, is to increase a voltage level and modify the DAB circuit to an input serial output parallel (ISOP) topology. It consists of cascaded H-Bridges on high-voltage side and their parallel connection on the low-voltage side. This approach is often utilized in a smart transformer applications [11]. There are a few other connections possible as mentioned in [12], however, an input parallel output parallel (IPOP) one is especially interesting [13]. This choice offers a simple solution to increase a system's total power capability. Moreover, such configuration provides following benefits: reliability improvement due to additional level of redundancy, simplicity of maintenance as whole module can be replaced, lowering manufacturing costs due to components standardization, more flexible converter design and reduced product development costs due to utilization of smaller modules, as well as simplified system reconfiguration, as mentioned in [14] and [15]. Finally, it is worth mentioning that the DAB module may be easily disconnected from operation by setting zero signals to all its switches, which allows to avoid any additional circuit modifications and significantly reduces losses of this idle state.

Thus, the IPOP DAB approach seems to be an interesting solution to increase HESS power capability. However, a problem of efficiency at light-loads conditions persists. Although it is undertaken in literature, in most cases it considers a single converter system and the most common approach to tackle this issue is by the DAB's phase-shift modulation modification as presented, e.g., in [16] and [17]. A number of papers presents approaches where similar improvements may be obtained by the DAB's topology modifications [18]–[22], e.g., by additional

Manuscript received January 3, 2019; revised April 16, 2019, July 1, 2019, and September 3, 2019; accepted October 25, 2019. Date of publication November 5, 2019; date of current version February 20, 2020. This work was supported by the TEAM-TECH/2016-1/5 Project carried out within the TEAM-TECH program of the Foundation for Polish Science co-financed by the European Union under the European Regional Development Fund. Recommended for publication by Associate Editor A. K. Gupta. *(Corresponding author: Michal Rolak.)*

The authors are with the Department of Electrical Engineering, Warsaw University of Technology, 00-662 Warsaw, Poland (e-mail: michal.rolak@ee.pw.edu.pl; sobolc@ee.pw.edu.pl; malin@isep.pw.edu.pl; stynskis@ee.pw.edu.pl).

Color versions of one or more of the figures in this article are available online at http://ieeexplore.ieee.org.

Digital Object Identifier 10.1109/TPEL.2019.2951833

transformer tap, or by application of variable inductor, etc. Another interesting literature study of DAB converter modified operation is presented in [23] where varying switching frequency mode, burst operation, and other methods are discussed. There are several papers that undertake this problem in the IPOP and ISOP systems as well, and they proposed similar solutions. Topology and modulation changes are introduced in order to improve the overall efficiency [11], [14], [15], [23], [24]. Additionally, the parallel IPOP configuration gives an opportunity for a number of optimization methods utilizing unequal power allocation between the modules. Papers [13], [25]–[28] present advanced algorithms for different converter types including: particle swarm optimization, genetic algorithms, etc. Strong emphasis is put on adequate current control method and proper communication between the modules [29], [30]. Finally, one of the simplest ways to optimize the IPOP system operation is to turn-ON and -OFF particular modules to increase the system efficiency. Some attempts were presented in [31] and [32]. Although, they describe cases of nonisolated and unidirectional converters.

However, none of the mentioned papers solve the optimization problem by showing how many modules, in the existing DAB IPOP system, should operate when at least two parameters of operating conditions (i.e., the ES's voltage level and different power demands) change. This problem should be tackled for all possible conditions considering energy flow direction. Therefore, this article presents an approach that allows to determine a number of simultaneously operating modules as a function of these two variables—which is a main contribution of this article. This article describes an example of a two-module DAB IPOP system, providing results in form of the optimal operating area obtained for different ESS voltage levels and power demand conditions, with the emphasis on maximization of total efficiency. Additionally, the proposed method includes finding proper initial control values allowing for switching between system configurations (i.e., number of operating modules) without any power changes. A proposed algorithm is based on parametric functions that require only single module input/output power curves as the input data. Next, the proposed method is validated on a detailed simulation model. Finally, an experimental study is performed in the laboratory to verify simulation results.

This article is organized as follows: Section II presents the two-module DAB IPOP topology and explains the problem in detail. Section III proposes a solution for the selection of optimal configuration. Section IV presents results obtained by a detailed simulation model; additionally, a validation method is introduced and tested. Automated bench test method and experimental validation of the proposed solution are shown in Section V. A summary is made in Section VI.

II. System Overview and Problem Description

A. System Overview

The IPOP connection of two identical DAB dc/dc converters is shown in Fig. 1. It must be stated that both H-bridges in each DAB module operate with rectangular voltage output waveform and 0.5 duty cycle assuring simple phase-shift control.

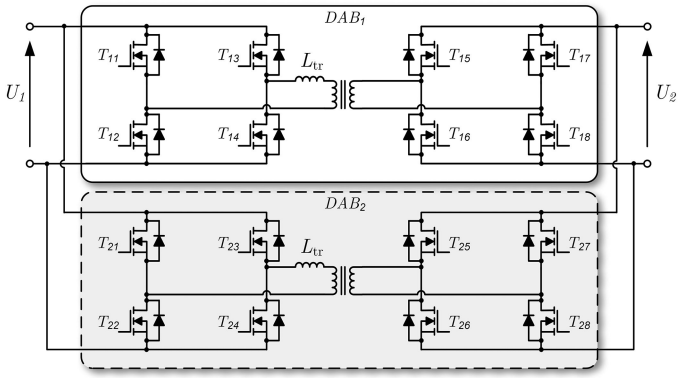

Fig. 1. General scheme of two-module IPOP DAB topology.

Power transferred by a single ideal module is described by the following:

$$P(\phi) = \frac{nU_1U_2\phi(\pi - |\phi|))}{2\pi^2 L_{\text{tr}} f_{\text{sw}}} \tag{1}$$

where: $P-$transferred power, $n-$transformer turns ratio, U_1-constant dc voltage, U_2-varying voltage of the ES, $L_{\text{tr}}-$corresponds to a total lumped leakage inductance of the high-frequency transformer and auxiliary inductance, $f_{\text{sw}}-$ is a switching frequency of the converter, and ϕ is a phase-shift between voltage waveforms generated by each of H-Bridge within single DAB module. The ϕ's sign defines a direction of energy transfer, and it is assumed that the positive sign corresponds to positive energy being delivered to charge the storage element, and negative sign corresponds to the discharging process. Furthermore, it may be noticed in (1) that the amount of energy transferred depends linearly on U_2 voltage, which is important for the dc-type ES with wide-range voltage changes. For further analysis, a per-unit value is introduced, which is calculated in reference to the maximum output power value of the single DAB module. Thus, the whole system offers a total maximum power of 2 p.u.

Unfortunately, (1) describes an ideal lossless model and its efficiency is not taken into account. Therefore, example power curves showing differences between nonideal (blue and red solid lines for p_{U_1} and p_{U_2}, respectively) and ideal (black dashed line) are presented in Fig. 2. They were obtained for U_2 rated voltage [see Fig. 2(a)], and half of the U_2 rated value [see Fig. 2(b)] to show that change in U_2 not only changes the output power but a ratio of the nonideal input/output curves which, in turn, affects the efficiency as well. The p_{U_1} and p_{U_2} are in fact the averaged power values of the U_1 and U_2 voltage sources, respectively. The p_{U_1} is an input quantity and the p_{U_2} is the output quantity when the DAB converter charges an ES, while p_{U_1} is the output and p_{U_2} is the input quantity when the converter operates in the discharging mode. Differences between the ideal and nonideal power curves shown in Fig. 2 result from detailed losses inclusion. This process is described in the further sections of this article. Having detailed input/output power curves that correspond to a real device is especially important for the presented optimization method.

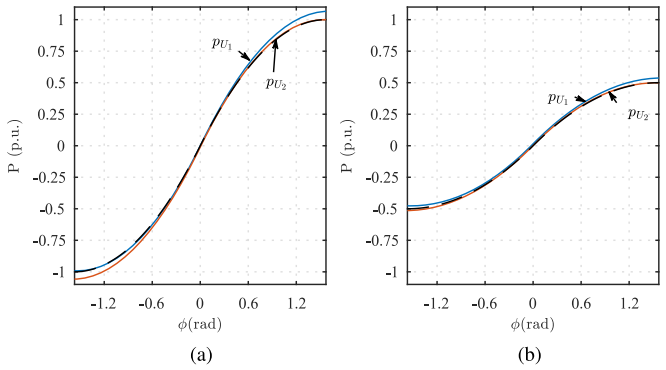

Fig. 2. Comparison of ideal (black dashed-line) and nonideal (p_{U_1}, p_{U_2}) power curves of a single DAB module for: (a) $U_2 = 1.0$ p.u.; (b) $U_2 = 0.5$ p.u., respectively.

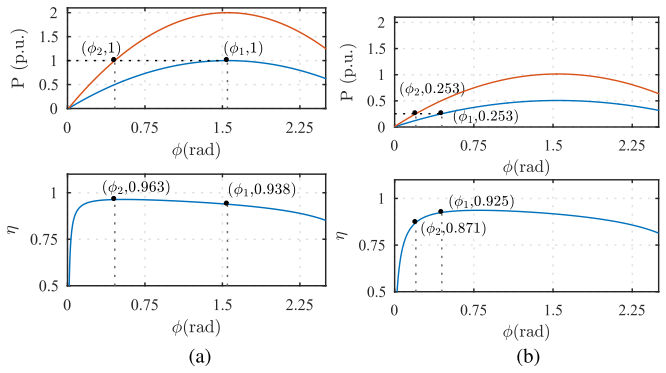

Fig. 3. IPOP DAB overall efficiency problem illustration. Power curves of 1×DAB (blue line) and 2×DAB (red line), and efficiency curves for: (a) $U_2 = 1.0$ p.u., and (b) $U_2 = 0.5$ p.u., respectively.

B. Problem Description

To clearly illustrate a problem of optimal configuration selection the output power and efficiency curves are shown in Fig. 3. They are presented for the positive ϕ phase-shift values (ES's charging) at rated [see Fig. 3(a)] and half of the rated ES's voltage [see Fig. 3(b)], respectively. The top graphs present the output power curves of the single-module (blue)—and will be further denoted as 1×DAB, and two-modules in parallel (marked in red)—that will be further denoted as 2×DAB. The bottom graphs present efficiency curves of single DAB module for two different U_2 voltages. As mentioned before, here it may be observed that the efficiency function changes not only with the phase-shift value but in reference to the ES's voltage as well. When both modules operate with equal phase-shift the total maximum power equals 2 p.u. but there is only single efficiency function as all the modules are the same.

Here, it may be observed that for a case where IPOP system demands power level of 1 p.u. at rated voltage value [see Fig. 3(a)], there are two possible solutions: first—where 2×DAB operate with ϕ_2 phase shift; second—where 1×DAB operates with ϕ_1 whose value is greater than the ϕ_2. While both cases assure the same power level they operate with different efficiencies of 96.3% and 93.8%, respectively. Thus, it is recommended to operate with 2×DAB in these conditions. An opposite situation takes place for $U_2 = 0.5$ p.u. and $P = 0.25$ p.u. shown in Fig. 3(b). It may be noticed that for these operating conditions, it is more efficient to use 1×DAB with ϕ_1 phase-shift and 92.5% efficiency instead of 2×DAB with 87.1% efficiency.

As both loading power (P) and ES's voltage level (U_2) vary during the system operation, the operating point change may be addressed by finding the optimal number of working modules that assures the highest available efficiency for given operating conditions. The problem can be defined as a function returning the number of working modules k out of the total parallel modules m in the system, and for the considered case (i.e., $m = 2$) it may be described as follows:

$$F(U_2, P) = \{k : \eta_k = \max(\eta_1(U_2, P), \eta_2(U_2, P))\} \quad (2)$$

where

$$\eta_k = \frac{p_{k,\text{out}}}{p_{k,\text{in}}} \quad (3)$$

and as mentioned before the $p_{k,\text{out}}$ and $p_{k,\text{in}}$ can swap places in accordance with the energy flow direction. Moreover, when a bidirectional operation is considered the solution is limited to the following operational conditions:

$$\begin{aligned} U_2 &\in (0, 1\rangle \\ P &\in \langle -2, 0) \cup (0, 2\rangle \end{aligned} \quad (4)$$

where the 0 values are excluded due to lack of energy transfer. In addition to obtaining the k number, an adequate pair of $\phi_{k,\text{stop}}$ and $\phi_{k+1,\text{ start}}$ values has to be found for each corresponding k value. This is to allow for starting the configuration of $(k+1)$th converters at the same instant (power level) that stops the kth configuration. Any transient states of particular setup are beyond the scope of this article.

III. Problem Solution

A problem solution—that assures all the unknowns discussed in Section II—may be found by searching for intersection points of parametric curves traced for different voltage U_2 levels. It can be derived, that for given U_2's voltage level parametric equations of each system's configuration may be expressed as follows:

$$h_k(\phi) = \begin{cases} x = p_{k,\text{out}}(\phi) \\ y = \eta_k(\phi) \end{cases} \quad (5)$$

where ϕ is the phase-shift parameter. Fig. 4 (plotted for an arbitrary input/output power functions) illustrates this idea showing (5) for two parallel modules. It shows the positive ϕ values at $U_2 = 1$ p.u. [see Fig. 4(a)] and $U_2 = 0.5$ p.u. [see Fig. 4(b)], respectively. Arrows indicate increase of the ϕ phase-shift. It may be observed in what power range (denoted with $k = 1$) the single module offers higher efficiency. Similarly, the operation range for two-modules performing together is denoted with $k = 2$. It has to be mentioned that the intersection X point's coordinates are common for the h_1 and h_2 functions, but parameters ϕ for each curve is different. For instance, for the h_1 it is a phase-shift value that the single module should stop to operate at, and may be denoted as $\phi_{1,\text{stop}}$. Furthermore, for the h_2 it describes an initial

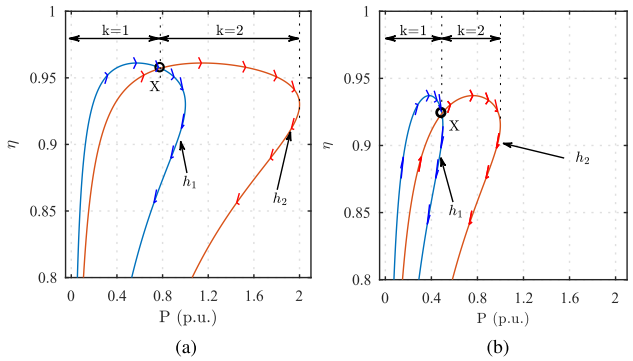

Fig. 4. Arbitrary parametric functions illustrating the proposed method for following system configurations: 1×DAB (blue) and 2×DAB (red) which are plotted for: (a) $U_2 = 1.0$ p.u., and (b) $U_2 = 0.5$ p.u., respectively.

phase-shift value (named $\phi_{2,\text{start}}$) that two-modules should start to operate at, in order to continue the power increase from the value the 1×DAB stopped at.

The most challenging issue in this approach is to introduce analytical equations for the power and efficiency functions. Some attempts can be found in [7], however, it provides significantly complex equations that resulted from symbolic solver. Additionally, these equations include only inductors' and MOSFETS' resistances. On the other hand, the efficiency function may be obtained by power losses estimation using the second-order polynomial approximation as presented in [25]–[27], [30], [33]. Obtained polynomial's coefficients correspond to: constant losses (e.g., control power), linearly dependent losses (e.g., diode's conduction losses), and quadratically dependent losses (e.g., MOSFET's resistance losses). However, additional nonlinearities caused by, e.g., switching losses are neglected and they are especially important for the DAB topology operating outside of the zero voltage switching region [34], what is typical for varying U_2 voltage level. Nonetheless, the proposed method is based on the approximation of a single module's input/output power curves, and not on the module's losses, and may be presented as an Nth order polynomial approximation with phase-shift as a variable

$$p_{U_1}(\phi) = a_N\phi^N + a_{N-1}\phi^{N-1} + \cdots + a_1\phi + a_0 \quad (6)$$

$$p_{U_2}(\phi) = b_N\phi^N + b_{N-1}\phi^{N-1} + \cdots + b_1\phi + b_0 \quad (7)$$

It may be noticed that a power equation of the DAB (1) is already a second-order function and it is a lossless model. Then, to verify the proposed approach, within this article, the $N = 3$ order is used as the smallest possible polynomial's order that can include additional nonlinearities resulting from losses. Finally, the efficiency function may be expressed as follows:

$$\eta(\phi) = \begin{cases} p_{U_2}(\phi)/p_{U_1}(\phi) & \text{for charging the ES} \\ p_{U_1}(\phi)/p_{U_2}(\phi) & \text{for discharging the ES} \end{cases} \quad (8)$$

this is due to bidirectional energy transfer ability of the power converter. Having all functions dependent on single ϕ phase-shift variable, and assuming that all parallel converters are the same, it is now possible to use the parametric functions (5) to find optimal configuration for given operational conditions. Here, it

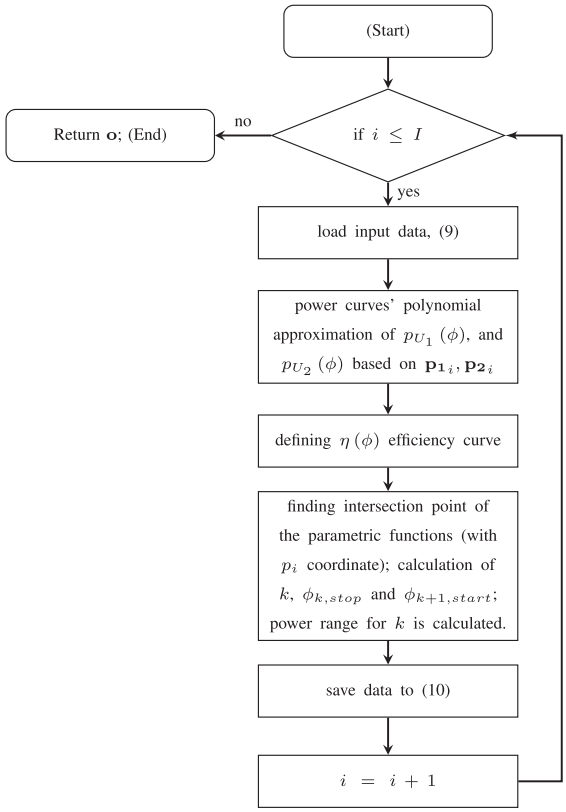

Fig. 5. Flow chart diagram for the algorithm which finds optimal configuration selection in the two-module IPOP DAB converter system.

is stressed, that due to chosen polynomials order and presence of these polynomials' quotients a numerical methods are utilized to find the intersection points.

As mentioned before, system's power, and thus its efficiency curves strongly depend on the U_2 voltage. First of all, the necessary data (i.e., input/output power curves) of the single module have to be collected for different voltage levels. This may be done by measuring these quantities with J resolution of ϕ phase-shift values for I different voltage levels; both the I and J numbers are integer values. Then, an input data structure consists of

$$\mathbf{v}_i = \left[\mathbf{p_1}_{1\times J}\mathbf{p_2}_{1\times J}\right]^T, u_i = i/I \quad (9)$$

where: $\mathbf{p_1}$ and $\mathbf{p_2}$ of length J are the sampled U_1 and U_2 voltage values at averaged power level, and u_i is the U_2 voltage value for ith voltage level. The values that are being searched may be presented as the output vector that is defined as follows:

$$\mathbf{o}_i = [k\ \phi_{k,\text{stop}}\ \phi_{k+1,\text{ start}}\ u_i\ p_i] \quad (10)$$

where: $i = 1, 2, \ldots, I$ and p_i is a power coordinate of the intersection point, that along with u_i, are required by (2).

Then, for each voltage level the polynomial approximation has to be performed separately for charging and discharging modes. This allows to define the efficiency function, and in turn, the parametric functions for different systems configurations. Having the parametric functions, it is now possible to find the

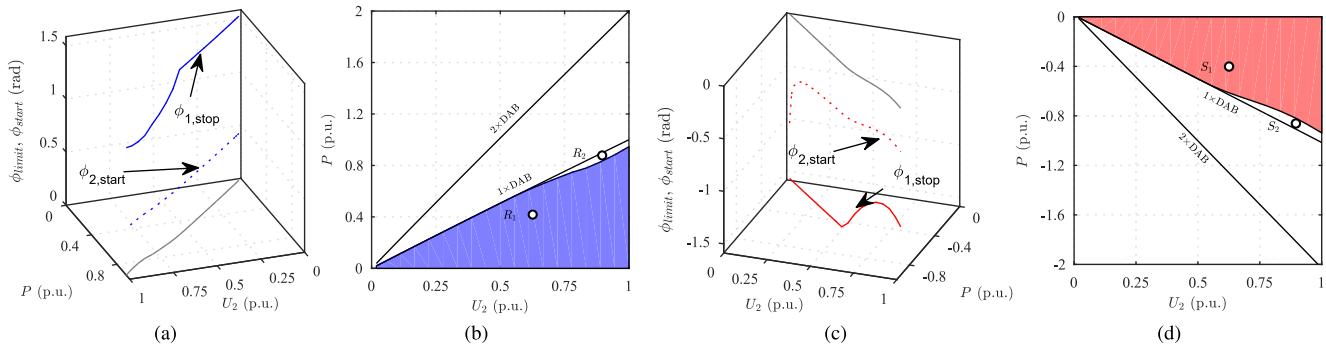

Fig. 6. Optimization method results based on the simulation model for two-module DAB IPOP converter: (a) Three-dimensional (3-D) curves of $\phi_{1,\text{stop}}$ and $\phi_{2,\text{start}}$ for charging operation; (b) $P-U_2$ projection of $\phi_{1,\text{stop}}$ for charging operation resulting in optimized area for $k=1$ (blue area); (c) 3-D curves $\phi_{1,\text{stop}}$ and $\phi_{2,\text{start}}$ for discharging operation; (d) $P-U_2$ projection of $\phi_{1,\text{stop}}$ for discharging operation resulting in optimized area for $k=1$ (red area).

intersection point that allows to determine which system's configuration assures best efficiency in given power ranges. Finally, it is required to calculate the $\phi_{1,\text{stop}}$ and $\phi_{2,\text{start}}$, respectively, and save all the data to the output vector. Proposed approach may be addressed in a form of an algorithm shown in Fig. 5. It is worth to stress that power curves of a real converter's module change in a long-run due to components' aging, and may require periodic updates of the optimized operating areas.

IV. Simulation Study

To conduct the optimal configuration selection analysis non-ideal power curves of a single DAB's module model are collected for different ES voltages and saved in sets. Calculated operation range should be verified with a proper testing method performed independently on 1×DAB and 2×DAB simulation models, respectively. Proposed validation method is also tested in this section to ensure its correctness for further laboratory research.

A. Model

A simulation model was built in PLECS software and includes transformer magnetizing inductance L_m, transformer's core losses modeled as resistor R_m parallel to L_m, and switching losses. It is worth noting that transformer's winding and auxiliary inductance's resistances are lumped together as R_{tr} similarly to the transformer's leakage inductances L_σ combined with auxiliary inductor into L_{tr}. A complete list of the model's parameters is shown in Table I in the Appendix. Important factors such as conduction losses of the temperature dependent MOSFETS' channel resistance and switching losses, are calculated from a detailed manufacturer's models in a form of adequate look-up tables [35]. Additionally, a SiC diode losses are modeled according to the manufacturer's library [36]. Due to temperature dependent parameters thermal steady-states simulations are required to be performed for every operating point.

B. Simulation-Based Analysis

For the analysis, a set of 30 ($J=30$) discrete ϕ phase-shift angles are subsequently generated within a range $[-15/18\pi, +15/18\pi]$ for every of 18 ($I=18$) U_2 voltage levels. This low value of the measurements' resolution is chosen to reflect experimental conditions assuring a reasonable tests duration.

Performing the optimization algorithm (e.g., in MATLAB software) presented in Fig. 5 on the datasets taken from the simulation circuit results in final solutions presented in Fig. 6. Pairs of figures [see Fig. 6(a) and (b)] and [see Fig. 6(c) and (d)] correspond to the charging and discharging operation modes, respectively. The 3-D solid lines [see Fig. 6(a) and (c)] present the $\phi_{1,\text{stop}}$ with regards to varying power (P) and U_2 voltage. This indicates at what phase-shift value (z-axis) 1×DAB should be replaced by 2×DAB operation. Additionally, the colored dashed-lines represent the $\phi_{2,\text{start}}$ values. The gray lines are the $\phi_{1,\text{stop}}$ projections on the $P-U_2$ planes. Fig. 6(b) and (d) presents the solutions in so called top-view, and show the operation range (blue and red areas corresponding to $k=1$) for 1×DAB that has higher efficiency than two modules, and it is limited by 3-D curve projection on $P-U_2$ plane and the U_2–axis. The remaining area (i.e., between colored region and the 2×DAB black solid line) corresponds to area where $k=2$ configuration allows to achieve higher efficiency. The black solid lines labeled 1×DAB and 2×DAB show maximum power values for different U_2 for particular modules' configurations. It may be observed that the maximum power of each configuration increases linearly with the U_2 voltage, what agrees with (1). Furthermore, it may be observed in Fig. 6(b) that for the operation point R_1 ($P=0.41$, $U_2=0.63$) it is better to operate with 1×DAB instead of 2×DAB. It is reasonable as the operating power is within range of single converter. However, if the operating point is R_2 ($P=0.87$, $U_2=0.9$) it is more efficient to use 2×DAB instead of single module. This is counterintuitive as this power is still within single module's power range. Similar reasoning may be conducted for the S_1 and S_2 operating points for the ES discharging operation presented in Fig. 6(d).

C. Simulation-Based Validation

Proposed analysis method is based on a fact that in multi-module IPOP dc/dc converter consisted of identical devices, an optimized operation region may be obtained from power

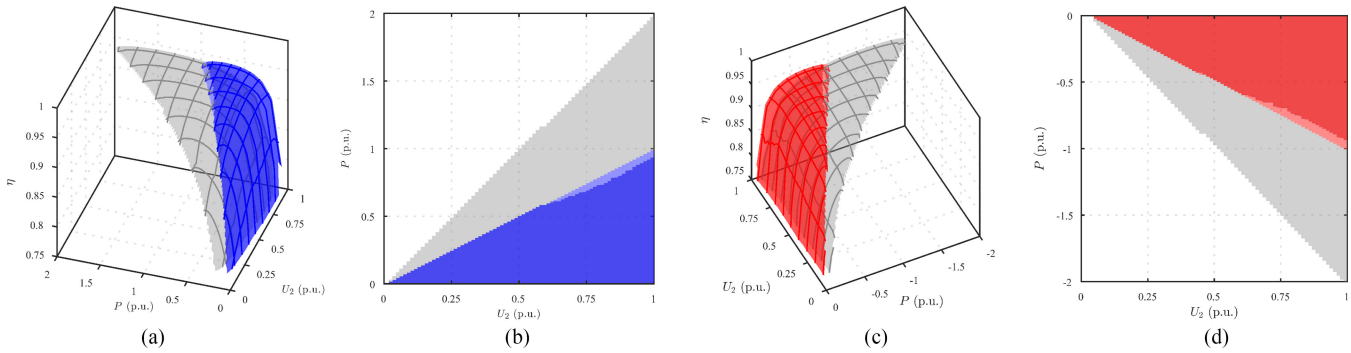

Fig. 7. Validation method's results of the simulated model for optimized IPOP DAB operation: (a) efficiency surfaces for 1×DAB (blue) and 2×DAB (gray) for the ES charging; (b) top-view of the Fig. 7(a); (c) efficiency surfaces for 1×DAB (red) and 2×DAB (gray) for the ES discharging; (d) top-view of the Fig. 7(c).

functions of a single module. Then, an open-loop validation method is introduced to examine the solution. It is important for this method to be easily applied for the real test-bench validation during a laboratory experiment. This method uses simple efficiency measurements for varying P (obtained by changing the phase-shift) and U_2 voltage as performed separately for 1×DAB and 2×DAB configurations. This may be done by performing phase-shift "sweep" (including steady state, however) for each U_2 voltage level and by plotting efficiency surfaces. In Fig. 7, the two-module operation is depicted in gray, and single module performance is denoted with color (blue and red for the ES charging and discharging, respectively). The number of measured points is the same as for the previous analysis—that is 18 power characteristics of 30 phase-shift samples each. Due to constant samples number for every U_2 voltage, the collected data points (not displayed to show uncluttered figures) have to be interpolated with computational software in order to obtain efficiency surfaces. Fig. 7(a) and (c) presents surface-to-surface intersections for charging and discharging operation, respectively. For sake of clarity Fig. 7(b) and (d) shows the solutions' top-views that allow to inspect the operation area obtained analytically. Surfaces' colors were set to different levels of transparency to illustrate their intersections. It may be observed that the Fig. 7(b) confirms the prediction of Fig. 6(b) as well as the Fig. 7(d) matches with Fig. 6(d). Worth stating is a fact, that the area's regions close to U_2 axis were colored for sake of clarity, because the energy flow direction's change does not occur at constant $\phi = 0$ value but varies with changing ES' voltage. Nonetheless, the convergence of analytical results and the output of independent validation technique allows to assume that the proposed method for optimal configuration selection is correct.

V. Experimental Results

A. Automated Test-Bench

Two modules were built to validate the proposed approach. One of which is shown in Fig. 8. Every converter's switch consists of two C3M0065090 J SiC MOSFETs connected in parallel to reduce channel's resistance. Additionally, to avoid a high forward voltage drop of the MOSFET's body diode

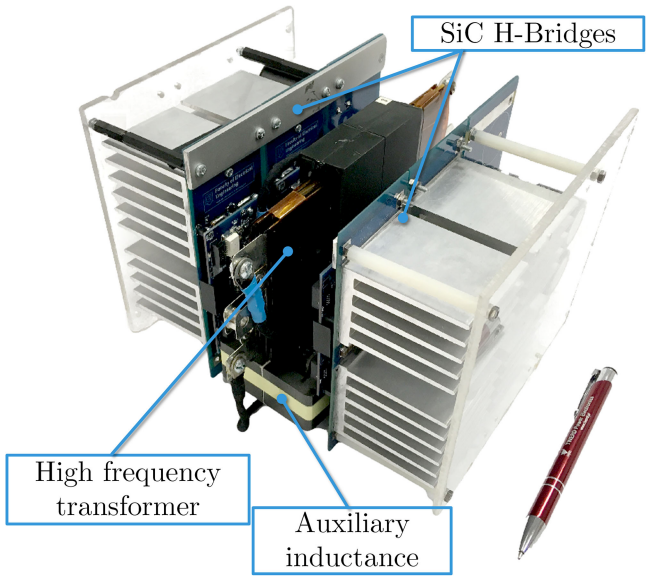

Fig. 8. Single DAB module build for the experimental test-bench.

the external STPSC6H065 freewheeling SiC diode is used. The auxiliary inductance equals $L_{\text{aux}} = 62\ \mu$H. Parameters of the laboratory single DAB converter are listed in Table I of the Appendix and correspond to the simulation ones.

To collect real-power curves of the single DAB module, and for further validation process, an appropriate test bench is required. A general scheme of the two module, IPOP DAB laboratory setup is presented in Fig. 9. It consists of two main parts: control/measuring circuit and power circuit. Control signals for the converters are delivered by TMS320F28379 microcontroller that is connected to the MATLAB software through the MODBUS protocol. Moreover, this software is also used as acquisition tool—logging $i_1(t)$, $u_1(t)$ and $i_2(t)$ and $u_2(t)$ (from a power analyzer), which are required for the p_{U_1} and p_{U_2} approximation.

Proposed test-bench scheme is a result of low operating voltage test conditions of the system, where U_1 equal to 270 V U_2 and varies from 0 to 270 V. This resulted in the inability to use of commercially available active rectifiers. Then, two

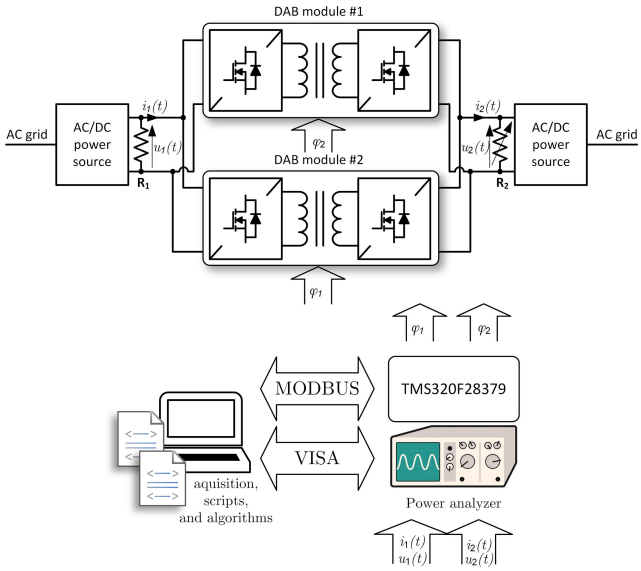

Fig. 9. General scheme of the two-module DAB IPOP laboratory test-bench.

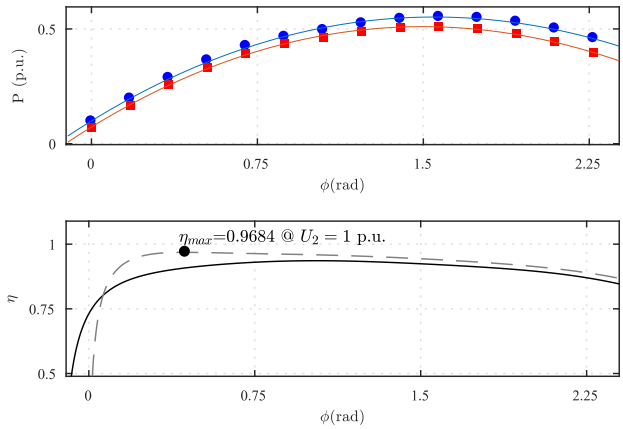

Fig. 10. Example of experimental input data obtained from the single DAB module. Top graph: input/output power curves data with the 3rd polynomial approximation. Bottom graph: module's efficiency curves obtained for $U_2 = 0.5$ p.u. (solid black line) and for $U_2 = 1.0$ p.u. (gray dashed line).

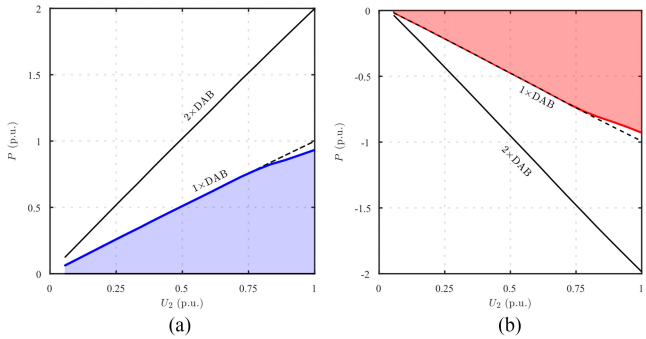

Fig. 11. Provided solution (colored area) based on 540 samples points obtained from experimental power curves of the single DAB module for: (a) charging and (b) discharging mode, respectively.

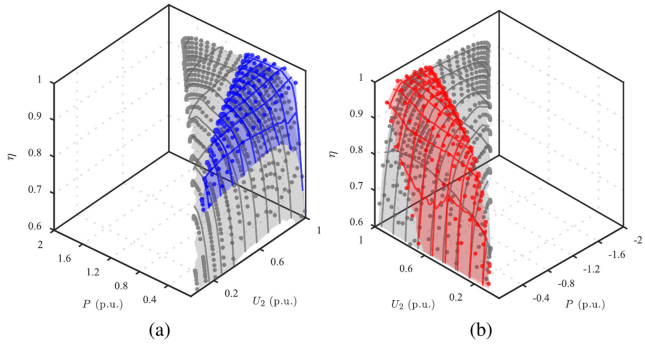

Fig. 12. Validation method's results on the experimental test-bench for 1×DAB (colored) and 2×DAB (gray) operation with surface interpolation of 540 samples points for: (a) charging, and (b) discharging operation mode, respectively.

programmable ac/dc industrial power supplies with parallel resistors R_1 and R_2 on their outputs were used. This connection assures a constant current across the resistors, which allows for bidirectional energy transfer of the DAB converters. The U_1 voltage source's loading increases when the ES is being charged and the U_2 becomes unloaded to keep the R_2 current constant. For the ES's discharging process, the situation is opposite. If the R_2 resistor is a rheostat with remotely changed resistance, the required datasets (similarly to the efficiency surfaces) may be easily collected in a fully automated process.

B. Experiment-Based Validation

In order to calculate optimal operating area, it is necessary to obtain power curves of single DAB module. Again, the same measurement resolution of 18 voltage levels, and 30 phase-shift points were utilized in order to shorten the experiment's duration time. The top graph of the Fig. 10 shows a 3rd order polynomial approximations (solid lines) of the single module's input/output power curves. Samples are measured for the ES charging operation at $U_2 = 0.5$ p.u. conditions. Acquired samples are denoted with ∘ and □ for $\mathbf{p_1}, \mathbf{p_2}$ vectors, respectively. The bottom graph shows the efficiency function (solid black line) for the considered $U_2 = 0.5$ p.u. voltage. An additional gray dashed-line shows the efficiency curve for the ES voltage of $U_2 = 1$ p.u. to present the single module's maximum efficiency of 96.84%.

The final solution, based on the real test-bench power curves is shown in Fig. 11. Fig. 11(a) and (b) presents obtained operation regions for ES's charging and discharging, respectively.

Finally, the open-loop validation method may be applied to verify the calculated solution. The results are presented in Fig. 12 as the efficiency surfaces for the ES charging and discharging operation. In this case, the measured data points are marked explicitly. For more detailed results' presentation their top-views are shown in Fig. 13(a) and (b), respectively. Again, it may be observed that for a chosen condition such, e.g., $R_2 (P = 0.8$ p.u., $U_2 = 0.9$ p.u.) an operation of 2×DAB may be advised to obtain higher efficiency. It is important that this point is within a single module's power range. On the other hand, for lower values of the ES voltage range it is advised to utilize 1×DAB up to its maximum power before switching into 2×DAB operation.

It is easy to notice that the 2×DAB operation does not reach 2 p.u. power for rated U_2 voltage. This may be a result of

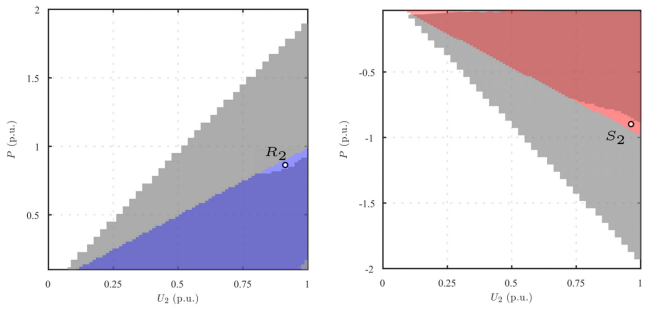

(a) (b)

Fig. 13. Top-view of the Fig. 12: (a) Charging. (b) discharging the ES, respectively.

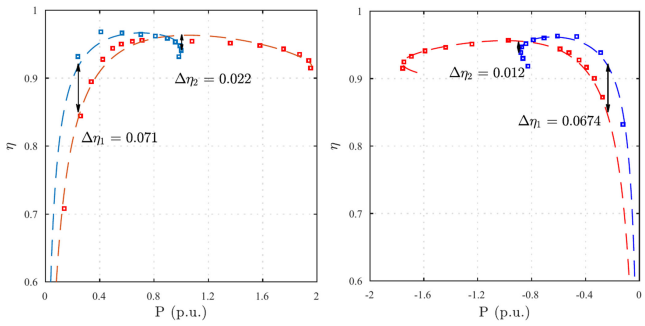

(a) (b)

Fig. 14. Efficiency improvement for a single (blue) and two-module (red) DAB converters for the: (a) charging operation at $U_2 = 1.0$ p.u.; (b) discharging operation at $U_2 = 0.9$ p.u.

additional currents circulating between modules that have not been taken into account during simulation and analysis. Additionally, some inaccuracies may occur due to chosen measurement resolution and surfaces' interpolation.

Finally, a quantitative representation of the overall efficiency gain, for chosen voltage levels, is shown in Fig. 14 for charging [see Fig. 14(a)] and discharging [see Fig. 14(b)] modes, respectively. The blue color depicts the single module data, whereas the red one corresponds to the two-module configuration. Dashed lines overlaying measured points are the parametric functions obtained due to 3rd-order polynomial approximations of measured input/output power functions. The efficiency deltas were measured between those approximated curves. It may be observed that for charging operation $U_2 = 1$ p.u. (an arbitrary choice) in Fig. 14(a): for lower power's ranges such as for $P = 0.25$ p.u. a significant efficiency gain of 7.1% is obtained; on the other hand, at the maximum power of single converter ($P = 1$ p.u.) the efficiencies difference equals to 2.2%. For the discharging conditions at $U_2 = 0.9$ p.u. (an arbitrary choice): for the lower power level such, i.e., $P = -0.25$ p.u. the efficiencies' difference equals to 6.7%; on the other hand, the efficiency gain for $P = -0.9$ p.u. equals 1.2%. Some differences in input/output power curves approximation may be noticed for those two cases, what suggests to pay more attention of the polynomial approximation order for larger U_2 values.

VI. Conclusion

An IPOP connection of DAB dc/dc converters is a suitable solution for increased power requirements of ESS applications, where high power demands occur together with wide range voltage changes (as in, e.g., hybrid energy storage). Additionally, they offer beneficial, but simple and cost-effective, solution for maximizing efficiency in different operating conditions that may be obtained by turning-ON and -OFF particular modules without any additional circuit and control algorithm modification.

This article proposes a method for defining at which operating conditions one or two DAB modules should operate together in order to fully utilize the existing DAB IPOP system and maximize its overall efficiency. The proposed method delivers a solution for a two-variable problem as the wide-range ES voltage changes and a full range of demanded power have to be taken into consideration including the bidirectional energy transfer. Described approach bases on polynomials' approximation of a single DAB's input/output power curves that are applied into parametric functions. The solution clearly indicates where a single module offers a higher efficiency than two-modules sharing power equally. The presented approach was successfully validated, at first, by the detailed simulation models, and followed by the laboratory tests performed on the test-bench consisted of two 1.4 kW SiC-based DAB converters operating at 100 kHz switching frequency.

Obtained results showed that for a wide range of voltages (from 0 to about 0.8 p.u.) it is more efficient to fully utilize a single DAB module up to its maximum power, instead of sharing it between the two modules. This operation region refers mainly to the supercapacitor-type ES, where significant voltage changes are possible. On the other hand, interesting results were found, that at the ES's voltage close to its rated value, there is an area of operating conditions (within the single module's power range), where two-modules should be employed to achieve higher efficiency. This is especially important for the battery-type ES, where voltage does not change in a wide range.

Appendix

See Table I.

TABLE I
Simulation and Experimental Single DAB's Parameters

Parameter	Symbol	Value	Unit
HV voltage	U_1	270	V
Energy Storage voltage range	U_2	0 to 270	V
Switching frequency	f_{sw}	100	kHz
Lumped inductance	L_{tr}	64	μH
Auxiliary inductance	L_{tr}	62	μH
Lumped resistance	R_{tr}	0.3	Ω
Magnetizing inductance	L_m	.7	H
Core losses	R_m	3500	Ω
Transformer winding ratio	n	1:1	$(-)$
Single DAB's max. power	P_n	1389	W
MOSFET's gate resistor	R_g	4	Ω

REFERENCES

[1] T. Dragi and J. M. Guerrero, "DC Microgrids—Part II: A review of power architectures, applications, and standardization issues," *IEEE Trans. Power Electron.*, vol. 31, no. 5, pp. 3528–3549, May 2016.

[2] I. Usera, P. Rodilla, S. Burger, I. Herrero, and C. Batlle, "The regulatory debate about energy storage systems: State of the art and open issues," *IEEE Power Energy Mag.*, vol. 15, no. 5, pp. 42–50, Sep./Oct. 2017.

[3] M. Lei *et al.*, "An MPC-based ESS control method for PV power smoothing applications," *IEEE Trans. Power Electron.*, vol. 33, no. 3, pp. 2136–2144, Mar. 2018.

[4] W. Jing, C. Hung Lai, S. H. W. Wong, and M. L. D. Wong, "Battery-supercapacitor hybrid energy storage system in standalone DC microgrids: A review," *IET Renew. Power Gener.*, vol. 11, no. 4, pp. 461–469, 2017.

[5] G. Buticchi, L. F. Costa, D. Barater, M. Liserre, and E. Dominguez, "A quadruple active bridge converter for the storage integration on the more electric aircraft," *IEEE Trans. Power Electron.*, vol. 33, no. 9, pp. 8174–8186, Sep. 2018.

[6] Y. F. Wang, L. K. Xue, C. S. Wang, and E. Al, "Interleaved high-conversion-ratio bidirectional DC–DC converter for distributed energy-storage systems-circuit generation, analysis, and design," *IEEE Trans. Power Electron.*, vol. 31, no. 8, pp. 5547–5561, Aug. 2016.

[7] F. Krismer, "Modeling and Optimization of Bidirectional Dual Active Bridge DC-DC Converter," Ph.D. dissertation, ETH Zurich, Zurich, Switzerland, 2010.

[8] N. Soltau, S. P. Engel, H. Stagge, and R. W. De Doncker, "Compensation of asymmetric transformers in high-power DC-DC converters," in *Proc. IEEE 5th IEEE Annu. Int. Energy Convers. Congr. Exhib*, 2013, pp. 1084–1090.

[9] Z. Li, Y. Wang, L. Shi, J. Huang, Y. Cui, and W. Lei, "Generalized averaging modeling and control strategy for three-phase dual-active-bridge DC-DC converters with three control variables," in *Proc. Conf. IEEE Appl. Power Electron. Conf. Expo.*, Tampa, FL, USA, 2017, pp. 1078–1084.

[10] G. Waltrich, M. A. M. Hendrix, and J. L. Duarte, "Three-phase bidirectional DC/DC converter with six inverter legs in parallel for EV applications," *IEEE Trans. Ind. Electron.*, vol. 63, no. 3, pp. 1372–1384, Mar. 2016.

[11] W. Qingshan and D. Liang, "Research on loss reduction of dual active bridge converter over wide load range for solid state transformer application," in *Proc. 11th Int. Conf. Ecol. Veh. Renew. Energies*, Monte Carlo, Monaco, 2016, pp. 1–9.

[12] P. Grzejszczak, R. Barlik, M. Nowak, and K. Wolski, "Bidirectional modular DC/DC converter for direct- current microgrids," in *Proc. Prog. Appl. Electr. Eng.*, Koscielisko, Poland, 2017.

[13] Y. Wang, F. Wang, Y. Lin, and T. Hao, "Sensorless parameter estimation and current- sharing strategy in two-phase and multiphase IPOP DAB DC DC converters," *IET Power Electron.*, vol. 11, no. 6, pp. 1135–1142, 2018.

[14] H. Fan and H. Li, "High-frequency transformer isolated bidirectional DC-DC converter modules with high efficiency over wide load range for 20 kVA solid-state transformer," *IEEE Trans. Power Electron.*, vol. 26, no. 12, pp. 3599–3608, Dec. 2011.

[15] Y. U. Du, A. Q. Huang, F. E. I. Xue, and M. C. Drive, "A modular integrated Li-ion battery pack with a multi-core based transformer isolated bidirectional DC-DC converter," in *Proc. 16th Eur. Conf. Power Electron. Appl.*, Lappeenranta, Finland, 2014, pp. 1–10.

[16] W. Choi, M. Lee, and B. H. Cho, "Fundamental duty modulation of dual-active-bridge converter for wide-range operation," *IEEE Trans. Power Electron.*, vol. 31, no. 6, pp. 4048–4064, Jun. 2016.

[17] A. Taylor, G. Liu, H. Bai, A. Brown, P. M. Johnson, and M. McAmmond, "Multiple-phase-shift control for a dual active bridge to secure zero-voltage switching and enhance light-load performance," *IEEE Trans. Power Electron.*, vol. 33, no. 6, pp. 4584–4588, Jun. 2018.

[18] Z. Zhang, Z. Ouyang, O. C. Thomsen, and M. A. E. Andersen, "Analysis and design of a bidirectional isolated DC-DC converter for fuel cells and supercapacitors hybrid system," *IEEE Trans. Power Electron.*, vol. 27, no. 2, pp. 848–859, Feb. 2012.

[19] S. M. Shiva, N. B. Y. Gorla, P. Das, and S. K. Panda, "Tap changing transformer based dual active bridge bi-directional DC-DC converter," in *Proc. 9th Int. Conf. Power Electron.*, Seoul, South Korea, 2015, pp. 2025–2030.

[20] S. S. Muthuraj, V. K. Kanakesh, P. Das, and S. K. Panda, "Triple phase shift control of an LLL tank based bidirectional dual active bridge converter," *IEEE Trans. Power Electron.*, vol. 32, no. 10, pp. 8035–8053, Oct. 2017.

[21] J. W. Kolar, R. M. Burkart, S. Member, and J. W. Kolar, "Comparative η-ρ-σ Pareto Optimization of Si and SiC Multilevel," *IEEE Trans. Power Electron.*, vol. 32, no. 7, pp. 5258–5270, Jul. 2017.

[22] F. Xue, R. Yu, and A. Q. Huang, "A 98.3% efficient GaN isolated bidirectional storage system applications," *IEEE Trans. Ind. Electron.*, vol. 64, no. 11, pp. 9094–9103, Nov. 2017.

[23] R. A. Abramson, S. J. Gunter, D. M. Otten, K. K. Afridi, and D. J. Perreault, "Design and evaluation of a reconfigurable stacked active bridge dc/dc converter for efficient wide load-range operation," in *Proc. IEEE Conf. Appl. Power Electron. Conf. Expo.,* 2017, pp. 3391–3401.

[24] T. Todorcevic, R. Van Kessel, P. Bauer, and J. A. Ferreira, "A modulation strategy for wide voltage output in DAB based DC-DC modular multilevel converter," *IEEE J. Emerg. Sel. Topics Power Electron.*, vol. 3, no. 4, pp. 4514–4520, Dec. 2015.

[25] G. Chen and X. Cai, "Adaptive control strategy for improving the efficiency and reliability of parallel wind power converters by optimizing power allocation," *IEEE Access*, vol. 6, pp. 6138–6148, 2018.

[26] J. Yan and L. Mu, "A method to improve the efficiency of asymmetric parallel converters for PV generation," in *Proc. 5th IEEE Int. Conf. Electr. Utility Deregulation, Restruct. Power Technol.*, 2016, pp. 1919–1923.

[27] F. H. Dupont, J. Zaragoza, C. Rech, and J. R. Pinheiro, "A new method to improve the total efficiency of parallel converters," in *Proc. Brazilian Power Electron. Conf..*, Gramado, Brazil, 2013, pp. 210–215.

[28] S. M. Shiva, N. B. Y. Gorla, P. Das, and S. K. Panda, "A new phase shedding and phase adding control scheme for interleaved DAB converter operating in IPOP configuration," in *Proc. INTELEC, Int. Telecommun. Energy Conf.*, Osaka, Japan, 2016, pp. 1–6.

[29] L. Yifei, W. Yubin, and W. Shanshan, "Sensorless current sharing in DC-DC converters," in *Proc. 18th Int. Conf. Electr. Mach. Syst.*, Pattaya, Thailand, 2015, pp. 1–6.

[30] S. Effler, M. Halton, K. Rinne, and A. C. Architectures, "Efficiency-based current distribution scheme for scalable digital power converters," *IEEE Trans. Power Electron.*, vol. 26, no. 4, pp. 1261–1269, Apr. 2011.

[31] S.-h. Baek, S.-R. Lee, and C.-Y. Won, "A novel phase shedding control algorithm considering maximum efficiency for 3-phase interleaved boost converter," in *Proc. IEEE Transp. Electrific. Conf. Expo, Asia-Pacific*, Busan, Korea, 2016, pp. 427–431.

[32] J.-T. Lin and K.-Y. Hu, "Digital Multiphase Buck Converter with Current Balance/Phase Shedding Control," in *Proc. IEEE Reg. 10 Conf.*, Macao, China, 2015, pp. 1–5.

[33] S. Wang, J. Liu, Z. Liu, T. Wu, and B. Liu, "Efficiency-based optimization of steady-state operating points for parallel source converters in stand-alone power system," in *Proc. IEEE 8th Int. Power Electron. Motion Control Conf.*, Hefei, China, 2016.

[34] R. T. Naayagi, A. J. Forsyth, and R. Shuttleworth, "Performance analysis of DAB DC-DC converter under zero voltage switching," in *Proc. 1st Int. Conf. Electr. Energy Syst.*, Newport Beach, CA, USA, 2011, pp. 56–61.

[35] Wolfspeed, Silicon Carbide Power MOSFET C3M Planar MOSFET Technology N-Channel Enhancement Mode. [Online]. Available: https://www.wolfspeed.com/c3m0065090j, Accessed on: Jun. 17, 2019.

[36] Wolfspeed., 10-A, 600-V, Z-Rec Schottky, TO-220 package. [Online]. Available: https://www.wolfspeed.com/c3d10060a, Accessed on: Jan. 6, 2016.

Michal Rolak received the M.Sc. degree in automatic control and robotics and Ph.D. degree in electrical engineering from the Institute of Control and Industrial Electronics, Warsaw University of Technology (WUT), Warsaw, Poland, in 2009 and 2016, respectively.

He is currently with the Institute of Control and Power Electronics, WUT. His current research interests include fault-tolerant algotihms for multiphase machines, ac/dc/ac back-to-back systems and optimized operation of multiple power converters for energy storages.

Cezary Sobol received the graduate degree from the Faculty of Electrical Engineering, Warsaw University of Technology, Warsaw, Poland, in 2018. Since October 2018, he has been working toward the doctoral degree at the Institute of Control and Power Electronics, Warsaw University of Technology.

He defended the M.Sc. thesis entitled: "Two parallel connected, isolated, bidirectional dc/dc (DAB type) converters—design, construction and efficiency analysis in various work conditions." He performed his research as a part of TEAM-TECH project entitled: "Highly efficient and fault tolerant SiC-based smart transformer in distributed energy systems." He is author and co-author of three papers in international journals and conferences. His research interests include bidirectional, isolated DC/DC converters for various applications (e.g., energy storages, smart transformer, etc.). Currently focuses on the topic of parallel connection of bidirectional, isolated dc/dc converters.

Mariusz Malinowski (S'99–M'03–SM'08–F'13) received the Ph.D. and D.Sc. degrees in electrical engineering from the Institute of Control and Industrial Electronics, Warsaw University of Technology (WUT), Warsaw, Poland, in 2001 and 2012, respectively.

He is currently with the Institute of Control and Industrial Electronics, WUT. He has coauthored more than 140 technical papers and seven books. His current research interests include the control and the modulation of grid-side converters, multilevel converters, smart grids, and power-generation systems based on renewable energies.

Prof. Malinowski was a recipient of the IEEE IES David Irwin Early Career Award, IEEE IES Bimal Bose Energy Systems Award, Polish Prime Minister Award and the Polish Ministry of Science and High Education Award.

Sebastian Stynski (S'06–M'12–SM'18) received the M.Sc. and Ph.D. degrees in electrical engineering from the Warsaw University of Technology (WUT), Warsaw, Poland, in 2006 and 2012, respectively.

Since 2013, he has been with the Institute of Control and Industrial Electronics, WUT, where he is currently an Assistant Professor. His research interests include modulation techniques and control methods of single and multiphase multilevel converters, resistance of power electronics systems on grid disturbances, power electronics interfaces between renewable energy sources and grid, and solid-state transformers.

Mr. Stynski was a recipient of the prestigious Scholarship (2014–2017) of Polish Ministry of Science and Higher Education for outstanding Young Scientists, in 2014. In recognition of outstanding achievements in development and implementation into industry of modulation and control methods for power electronics converters dedicated for the renewable power sources and mining industry, he was a Laureate of Scientific Team Award of the Rector of the WUT—the highest scientific award awarded annually by the WUT (2015) and a Laureate of the Prime Minister's 2017 I degree Team Award.